

Graph Neural Networks for the Prediction of Substrate-Specific Organic Reaction Conditions

Serim Ryou ^{*1} Michael R. Maser ^{*2} Alexander Y. Cui ^{*3} Travis J. DeLano ² Yisong Yue ³ Sarah E. Reisman ²

Abstract

We present a systematic investigation using graph neural networks (GNNs) to model organic chemical reactions. To do so, we prepared a dataset collection of four ubiquitous reactions from the organic chemistry literature. We evaluate seven different GNN architectures for classification tasks pertaining to the identification of experimental reagents and conditions. We find that models are able to identify specific graph features that affect reaction conditions and lead to accurate predictions. The results herein show great promise in advancing molecular machine learning.

1. Introduction

Graph neural networks (GNNs) have rapidly emerged as powerful predictive tools in the chemistry domain (Mater & Coote, 2019). Significant developments have been made in medicinal chemistry, where predictors of drug physicochemical properties (Coley et al., 2019; Withnall et al., 2020) and graph generative models (Elton et al., 2019; Blaschke et al., 2018) are readily available. Several examples have also been reported in organic synthesis, including for the classification of reaction types (Schwaller et al., 2019), the prediction of reaction products (Skoraczyski et al., 2017; Coley et al., 2017), and for retrosynthetic design (Segler et al., 2018; Coley et al., 2018). Despite the recent advancements, relatively few studies have been reported for the prediction of reaction conditions, arguably among the most challenging tasks chemists face (Coley et al., 2017).

Current deep neural networks (NNs) rely on multi-million

reaction training sets for sufficient data to make predictions in high-dimensional ($1,000^+$) label spaces (Gao et al., 2018). This offers flexibility in the reaction types that can be queried and includes a broad condition space from all of organic chemistry. However, given the sparsity of global datasets, reliable predictions are likely only obtained for the most common conditions of each reaction type, regardless of the structural differences between inputs. This poses a severe limitation for catalytic reactions in that the optimal conditions are often highly dependent on substrate structure (Mahatthananchai et al., 2012). It is therefore critical that deep networks distinguish between individual graphs of a reaction type when suggesting appropriate conditions to use.

To address the current limitations, we approach this prediction problem at the single reaction level. This allows for detailed learning of structure-condition relationships without the need to classify queries by learned reaction rules. We demonstrate the utility of our approach on curated datasets of four valuable reaction types from organic chemistry: Suzuki couplings (Miyaura & Suzuki, 1995), CN couplings (Bariwal & Van der Eycken, 2013), Negishi couplings (Negishi et al., 1977), and PausonKhand reactions (PKRs) (Khand et al., 1973). Our main contributions can be summarized as follows:

1. We apply domain expertise in dataset curation and in the construction of the label space.
2. We conduct a thorough assessment of modern GNN architectures, which, to our knowledge, has not yet been studied for models of chemical reactivity.
3. We achieve high accuracy in predicting condition vectors for all four datasets using strict evaluation metrics.
4. We provide an interpretability analysis to show the structural features informing our predictions.

2. Approach and Related Work

The work presented herein bears greatest similarity to Gao et al. (2018). In this report, a single GNN was trained on 12 million reactions from the full Reaxys database (Reaxys) for the task of predicting conditions. Product and reaction

^{*}Equal contribution ¹Computational Vision Lab, California Institute of Technology, Pasadena, California, USA ²Division of Chemistry and Chemical Engineering, California Institute of Technology, Pasadena, California, USA ³Department of Computing and Mathematical Sciences, California Institute of Technology, Pasadena, California, USA. Correspondence to: Michael R. Maser <mmaser@caltech.edu>, Sarah E. Reisman <reisman@caltech.edu>.

To appear in the ICML 2020 Workshop on Graph Representation Learning and Beyond (GRLB). Copyright 2020 by the author(s).

fingerprints (FPs) were used as inputs, where the latter was defined as the difference between the product and reactant graphs. Predictions were made in sequence for one possible catalyst, two solvents, and two reagents for all samples, regardless of reaction type. Intermediate predictions were concatenated as one-hot vectors with the FP inputs and passed to each subsequent layer, all of which were fully connected. Reasonable accuracies were obtained, though the inclusion of top-10 rankings and “close match” labels was required in many cases.

Our approach offers significant advantages over prior art on several accounts. We model focused reaction sets to obtain fine-grained, graph-specific predictions. Our networks take full graphs of all reaction components as inputs to minimize information loss in encoded structures. Our predictions use reaction-specific roles identified directly from dataset analysis to ensure proper chemical context of output vectors. We analyze only top-1 and top-3 predicted rankings to increase the feasibility of testing suggested results experimentally. We explicitly treat accuracies relative to a naive model to provide a rigorous evaluation framework. Even with these strict metrics, we obtain high accuracies through systematic testing of a suite of GNN architectures on each task.

3. Methods

Reaction data. Literature datasets are obtained from the Reaxys database and are pre-processed to remove incomplete records. A summary of the prepared datasets is included in Table 1. Detailed processing steps and data analysis can be found in the Supplementary Material (SM), including distributions of molecular properties, reaction yields, and reagent frequencies.¹ A general workflow for dataset preparation is as follows:

1. From Reaxys exports, SMILES string encodings (Weininger, 1988) of reactants and products are extracted for each data point.
2. Full condition vectors including reagents, catalysts, solvents, temperatures, etc. are extracted for each entry.
3. Dataset conditions are enumerated into dictionaries by reaction roles, which we term categories, and ground-truth vectors are binned accordingly.²

¹Since Reaxys is a subscription database, we are not permitted to publish exported data. We have compiled detailed procedures to prepare each dataset such that those with access can replicate our results. Most academic institutions have full-access Reaxys subscriptions. We make full reaction label dictionaries and all modeling code available at <https://github.com/slryou41/reaction-gcnn>.

²For consistency, individual reagents and conditions are referred to simply as labels, regardless of their identity. The terms label and bin are used interchangeably.

Table 1. Summary of reaction sets studied.

name	reactions	raw labels	bins	categories
Suzuki	145,413	3,315	118	5
CN	36,519	1,528	205	5
Negishi	6,391	492	105	5
PKR	2,749	335	83	8

With this procedure, significant trimming of the label spaces was achieved (see Table 1), while still maintaining deep and representative dictionaries.

Learning task & model setup. Similarly to Gao et al. (2018), we construct the learning problem as one of multi-label classification. Reactant and product graphs are fed as inputs to GNNs, which are trained to output binary condition vectors. The graphs are constructed using preprocessors from Chainer Chemistry (ChainerChem) (Tokui et al., 2015), which operate on RDKit mol objects (Open-Source, 2006) calculated from dataset SMILES.

Our modeling studies test seven GNN architectures from the ChainerChem library. Each model contains two sub-networks that are jointly trained for the overall task. The first subnet is a graph processing network (GPN) that differs between architectures and forms the basis of their relative performances. The GPNs convert input graphs to learned molecular embeddings, which are concatenated to form the overall reaction vectors. These are passed as input to the second subnet, a multilayer perceptron (MLP), for the ultimate predictions. GPNs explored in this work include neural fingerprinting networks (NFPs) (Duvenaud et al., 2015), gated graph sequence NNs (GGNNs) (Li et al., 2017), message passing NNs (MPNNs) (Gilmer et al., 2017), Weave module NNs (Weave) (Kearnes et al., 2016), relational graph attention networks (R-GATs) (Velickovi et al., 2018), relational graph convolutional networks (R-GCNs) (Schlichtkrull et al., 2017), and renormalized spectral graph convolutional networks (RS-GCNs) (Kipf & Welling, 2017).³ Models are trained for 100 epochs using the Adam optimizer (Kingma & Ba, 2017), sigmoid cross entropy loss, and an 80/10/10 train/validation/test split in all experiments. Further general modeling parameters and detailed hyperparameter settings for each model are included in the SM in Tables S2 and S3.

Model output and evaluation. We analyze the success of our models in terms of their accuracy in predicting the ground truth label for each reaction role. In practice, the outputs are simply probability vectors corresponding to the full reaction dictionaries. These are postprocessed by sort-

³Abbreviations used here are true to the original reports of each architecture; some differ from those in ChainerChem code.

Table 2. Summary of top-1 ranking accuracies for all architectures across the four datasets.

reaction	category	dummy	NFP	GGNN	MPNN	Weave	R-GAT	R-GCN	RS-GCN
Suzuki	AER	-	0.1572	0.1297	0.0259	0.0388	0.0801	0.2767	0.0750
	metal	0.3777	0.5763	0.5291	0.4513	0.4759	0.4891	0.6306	0.4987
	ligand	0.8722	0.8847	0.8811	0.8722	0.8724	0.8770	0.9036	0.8752
	base	0.3361	0.4637	0.4377	0.3494	0.3640	0.4167	0.5455	0.4052
	solvent	0.6377	0.6656	0.6656	0.6377	0.6381	0.6506	0.7049	0.6495
	additive	0.9511	0.9560	0.9563	0.9507	0.9507	0.9524	0.9624	0.9521
CN	AER	-	0.2575	0.3178	0.0453	0.1048	0.1983	0.3453	0.1821
	metal	0.2452	0.5485	0.5847	0.3304	0.4261	0.5082	0.5989	0.4792
	ligand	0.5219	0.6395	0.6789	0.5197	0.5327	0.6019	0.6981	0.5737
	base	0.2479	0.5340	0.5710	0.3227	0.3909	0.4753	0.5932	0.4721
	solvent	0.3219	0.4792	0.5348	0.3345	0.3690	0.4345	0.5647	0.4351
	additive	0.8904	0.8934	0.8978	0.8904	0.8907	0.8912	0.8984	0.8934
Negishi	AER	-	0.3071	0.4652	0.0916	0.0992	0.1539	0.4439	0.2228
	metal	0.2887	0.5470	0.6715	0.2887	0.3254	0.4067	0.6555	0.4833
	ligand	0.7879	0.8485	0.8708	0.7879	0.7879	0.7974	0.8724	0.8102
	temperature	0.3317	0.4864	0.6459	0.3732	0.4163	0.4035	0.6188	0.4864
	solvent	0.6938	0.8596	0.8852	0.8150	0.7911	0.8262	0.8868	0.8278
	additive	0.8309	0.8501	0.8820	0.8309	0.8309	0.8341	0.8724	0.8421
PKR	AER	-	0.2400	0.4377	-0.0294	0.1209	0.0825	0.3973	0.2265
	metal	0.4302	0.6340	0.7094	0.4302	0.4943	0.4566	0.7132	0.5774
	ligand	0.8792	0.8981	0.9094	0.8792	0.8868	0.8792	0.9057	0.9019
	temperature	0.2830	0.4415	0.6642	0.3358	0.4000	0.3283	0.6528	0.4755
	solvent	0.3321	0.5358	0.7396	0.3887	0.3774	0.4000	0.6792	0.5472
	activator	0.6906	0.7774	0.8679	0.6906	0.7094	0.6755	0.8415	0.7660
	CO (g)	0.7245	0.7849	0.8642	0.4755	0.6906	0.7208	0.8717	0.7434
	additive	0.9057	0.8943	0.8981	0.9057	0.9132	0.9057	0.8906	0.8981
	pressure	0.6528	0.8264	0.8679	0.8302	0.8415	0.8302	0.8491	0.8415

ing into categorical sub-dictionaries, and the final output is a list of labels for each category, ranked by their probability scores. A category’s prediction is classified as accurate if the ground truth label is identified in the model’s top- k predicted rankings. Here, we consider top-1 and top-3 predictions, though this is amenable to preference. Categorical accuracy (A_c) is defined as follows:

$$A_c = \frac{1}{N} \sum_{i=1}^N \mathbb{1}[P_i \cap Y_i] \quad (1)$$

where P_i and Y_i are the sets of predicted and ground truth labels of the i -th sample, respectively, and N is the number of samples in the test set (Wu & Zhou, 2017).

We directly compare model performances to a dummy predictor (dummy) that always suggests the most frequently occurring label(s) from each category of a dataset. Since

there is variable class-imbalance between categories (Cui et al., 2019) (see SM for full distributions), instead of averaging A_c values for a reaction model we calculate their average error reduction (AER) from baseline. We use AER to compare overall architecture performances on each task, and simply define it as follows:

$$\text{AER} = \frac{1}{C} \sum_{c=1}^C \frac{A_c^g - A_c^d}{1 - A_c^d} \quad (2)$$

where A_c^g and A_c^d are the accuracies of the graph network and dummy model in the c -th category, respectively, and C is the number of categories in the dataset dictionary.

4. Results and Analysis

The top-1 ranking accuracy of each architecture on all four tasks is presented in Table 2. An expanded results table

with top-3 performances is included in the SM in Table S4. Several of the tested networks provide strong general accuracy and significant AERs over baseline, with GGNNs and R-GCNs performing best in most cases. Categorical trends can be noted for each reaction, summarized below:

1. For the Suzuki dataset, when compared to baseline our models best improve metal and base predictions, but struggle with ligand and solvent.
2. For CN couplings, additives prove challenging, while good improvements are made otherwise.
3. For Negishi couplings, models perform very well with metal, temperature, and solvent predictions, but again struggle with additives.
4. For the PKR dataset, strong improvements are made with temperature, solvent, activator, and pressure, while only minor gains are seen for ligand and additive.

It is interesting to note that certain architectures behave differently between reactions, perhaps owing to model size, dataset size, and/or the chemical space within them. Though not included here, future studies will investigate the effects of specific convolution types in each architecture.

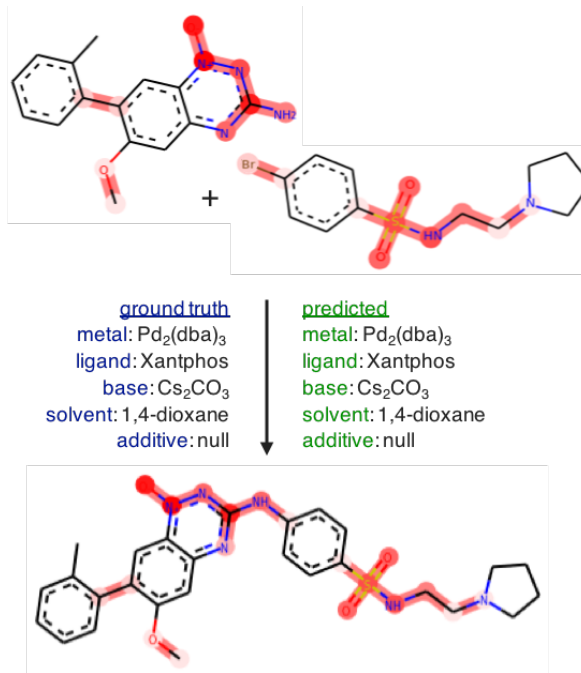
Model interpretation. To gain insight into the chemical information being learned in our modeling, we investigated the graph features leading to the observed predictions. To visualize groups of atoms most “informative” to the model readout, we extracted atom feature vectors from R-GCNs, the top performer from our modeling studies. An example visualization of a CN coupling is shown in Figure 1. In line with chemical intuition, the strongest activation comes from heteroatom (non-carbon) groups surrounding the reaction sites in the reactants and product. Additional activation is seen in distal groups that one might expect to interfere with the desired reaction. In this example, all five category labels are predicted correctly.

5. Discussion & Outlook

Advantages of the approach. As noted in Sections 1 and 2, the approach presented here has several major benefits:

1. Reaction-specific modeling offers fine-grained learning and circumvents the sparsity of out-of-scope reactions.
2. Expert-level label categorization ensures chemically reasonable outputs and reduces noise, a documented limitation of prior methods that we improve here.
3. Model readouts can be visualized, increasing the interpretability of molecular deep learning.

Figure 1. R-GCN activation visualization and predictions for a selected random reaction from the CN coupling test set. Darker highlights indicate higher atom activation.



Limitations. We also acknowledge certain limitations of the method. Since predictions are strictly structure-based, there is an inherent limit on the achievable accuracy. Several other features are expected to be informative for modeling what is really historical reaction data. Preliminary experiments have shown that metadata such as publication year does slightly increase model accuracy, but we exclude these features here since they have no physical bearing on reactivity. Further, we do not consider “close match” predictions. This results in more rigorous accuracy metrics, but discourages potentially useful conditions similar to the ground truth from being suggested. Altogether, we see several opportunities for improvement to be explored in future works.

Final remarks. In summary, we present a novel approach using GNNs to predict organic chemical reaction conditions. Categorizing labels by reaction role, we achieve top-1 ranking accuracies of up to 96% and reduce baseline error by as much as 47%. We find the approach general across four valuable reaction types, with GGNNs and R-GCNs performing well overall. Trained models can be readily applied to suggest context-specific experimental conditions, representing a significant contribution to synthetic chemistry. Ongoing work is focused on optimizing GNN architectures, adding to the available reaction types, and integrating label correlations in modeling. We expect the tools reported here to be of great value in molecular machine learning, including for computer-aided synthesis planning and drug development.

Acknowledgements

We thank the reviewers for their insightful comments and Prof Pietro Perona for mentorship guidance and helpful discussions on this work. Fellowship support was provided by the NSF (M.R.M., T.J.D. Grant No. DGE-1144469). S.E.R. is a Heritage Medical Research Investigator. Financial support from the Research Corporation Cottrell Scholars Program is acknowledged.

References

- Bariwal, J. and Van der Eycken, E. CN bond forming cross-coupling reactions: an overview. *Chemical Society Reviews*, 42(24):9283, 2013. ISSN 0306-0012, 1460-4744. doi: 10.1039/c3cs60228a. URL <http://xlink.rsc.org/?DOI=c3cs60228a>.
- Blaschke, T., Olivecrona, M., Engkvist, O., Bajorath, J., and Chen, H. Application of Generative Autoencoder in De Novo Molecular Design. *Molecular Informatics*, 37(1-2):1700123, 2018. ISSN 1868-1751. doi: 10.1002/minf.201700123. URL <https://onlinelibrary.wiley.com/doi/abs/10.1002/minf.201700123>.
- Coley, C. W., Barzilay, R., Jaakkola, T. S., Green, W. H., and Jensen, K. F. Prediction of Organic Reaction Outcomes Using Machine Learning. *ACS Central Science*, 3(5):434–443, May 2017. ISSN 2374-7943. doi: 10.1021/acscentsci.7b00064. URL <https://doi.org/10.1021/acscentsci.7b00064>.
- Coley, C. W., Green, W. H., and Jensen, K. F. Machine Learning in Computer-Aided Synthesis Planning. *Accounts of Chemical Research*, 51(5):1281–1289, May 2018. ISSN 0001-4842. doi: 10.1021/acs.accounts.8b00087. URL <https://doi.org/10.1021/acs.accounts.8b00087>.
- Coley, C. W., Jin, W., Rogers, L., Jamison, T. F., Jaakkola, T. S., Green, W. H., Barzilay, R., and Jensen, K. F. A graph-convolutional neural network model for the prediction of chemical reactivity. *Chemical Science*, 10(2):370–377, January 2019. ISSN 2041-6539. doi: 10.1039/C8SC04228D. URL <https://pubs.rsc.org/en/content/articlelanding/2019/sc/c8sc04228d>.
- Cui, Y., Jia, M., Lin, T.-Y., Song, Y., and Belongie, S. Class-Balanced Loss Based on Effective Number of Samples. *arXiv:1901.05555 [cs]*, January 2019. URL <http://arxiv.org/abs/1901.05555>. arXiv: 1901.05555.
- Duvenaud, D., Maclaurin, D., Aguilera-Iparraguirre, J., Gomez-Bombarelli, R., Hirzel, T., Aspuru-Guzik, A., and Adams, R. P. Convolutional Networks on Graphs for Learning Molecular Fingerprints. *arXiv:1509.09292 [cs, stat]*, November 2015. URL <http://arxiv.org/abs/1509.09292>. arXiv: 1509.09292.
- Elton, D. C., Boukouvalas, Z., Fuge, M. D., and Chung, P. W. Deep learning for molecular design: a review of the state of the art. *Molecular Systems Design & Engineering*, 4(4):828–849, 2019. ISSN 2058-9689. doi: 10.1039/C9ME00039A. URL <http://xlink.rsc.org/?DOI=C9ME00039A>.
- Gao, H., Struble, T. J., Coley, C. W., Wang, Y., Green, W. H., and Jensen, K. F. Using Machine Learning To Predict Suitable Conditions for Organic Reactions. *ACS Central Science*, 4(11):1465–1476, November 2018. ISSN 2374-7943. doi: 10.1021/acscentsci.8b00357. URL <https://doi.org/10.1021/acscentsci.8b00357>.
- Gilmer, J., Schoenholz, S. S., Riley, P. F., Vinyals, O., and Dahl, G. E. Neural Message Passing for Quantum Chemistry. *arXiv:1704.01212 [cs]*, June 2017. URL <http://arxiv.org/abs/1704.01212>. arXiv: 1704.01212.
- Kearnes, S., McCloskey, K., Berndl, M., Pande, V., and Riley, P. Molecular Graph Convolutions: Moving Beyond Fingerprints. *Journal of Computer-Aided Molecular Design*, 30(8):595–608, August 2016. ISSN 0920-654X, 1573-4951. doi: 10.1007/s10822-016-9938-8. URL <http://arxiv.org/abs/1603.00856>. arXiv: 1603.00856.
- Khand, I. U., Knox, G. R., Pauson, P. L., Watts, W. E., and Foreman, M. I. Organocobalt complexes. Part II. Reaction of acetylenehexacarbonyldicobalt complexes, (R1C2R2)Co2(CO)6, with norbornene and its derivatives. *Journal of the Chemical Society, Perkin Transactions 1*, 0(0):977–981, January 1973. ISSN 1364-5463. doi: 10.1039/P19730000977. URL <https://pubs.rsc.org/en/content/articlelanding/1973/p1/p19730000977>.
- Kingma, D. P. and Ba, J. Adam: A Method for Stochastic Optimization. *arXiv:1412.6980 [cs]*, January 2017. URL <http://arxiv.org/abs/1412.6980>. arXiv: 1412.6980.
- Kipf, T. N. and Welling, M. Semi-Supervised Classification with Graph Convolutional Networks. *arXiv:1609.02907 [cs, stat]*, February 2017. URL <http://arxiv.org/abs/1609.02907>. arXiv: 1609.02907.
- Li, Y., Tarlow, D., Brockschmidt, M., and Zemel, R. Gated Graph Sequence Neural Networks. *arXiv:1511.05493 [cs, stat]*, September 2017. URL <http://arxiv.org/abs/1511.05493>. arXiv: 1511.05493.

- Mahatthananchai, J., Dumas, A. M., and Bode, J. W. Catalytic Selective Synthesis. *Angewandte Chemie International Edition*, 51(44):10954–10990, October 2012. ISSN 14337851. doi: 10.1002/anie.201201787. URL <http://doi.wiley.com/10.1002/anie.201201787>.
- Mater, A. C. and Coote, M. L. Deep Learning in Chemistry. *Journal of Chemical Information and Modeling*, 59(6): 2545–2559, June 2019. ISSN 1549-9596, 1549-960X. doi: 10.1021/acs.jcim.9b00266. URL <https://pubs.acs.org/doi/10.1021/acs.jcim.9b00266>.
- Miyaura, N. and Suzuki, A. Palladium-Catalyzed Cross-Coupling Reactions of Organoboron Compounds. *Chemical Reviews*, 95(7):2457–2483, November 1995. ISSN 0009-2665, 1520-6890. doi: 10.1021/cr00039a007. URL <https://pubs.acs.org/doi/abs/10.1021/cr00039a007>.
- Negishi, E., King, A. O., and Okukado, N. Selective carbon-carbon bond formation via transition metal catalysis. 3. A highly selective synthesis of unsymmetrical biaryls and diarylmethanes by the nickel- or palladium-catalyzed reaction of aryl- and benzylzinc derivatives with aryl halides. *The Journal of Organic Chemistry*, 42(10):1821–1823, May 1977. ISSN 0022-3263, 1520-6904. doi: 10.1021/jo00430a041. URL <https://pubs.acs.org/doi/abs/10.1021/jo00430a041>.
- Open-Source. RDKit: Open-Source Cheminformatics Software, 2006.
- Reaxys. Reaxys. URL <https://new.reaxys.com/>.
- Schlichtkrull, M., Kipf, T. N., Bloem, P., Berg, R. v. d., Titov, I., and Welling, M. Modeling Relational Data with Graph Convolutional Networks. *arXiv:1703.06103 [cs, stat]*, October 2017. URL <http://arxiv.org/abs/1703.06103>. arXiv: 1703.06103.
- Schwaller, P., Probst, D., Vaucher, A. C., Nair, V. H., Laino, T., and Reymond, J.-L. Data-Driven Chemical Reaction Classification, Fingerprinting and Clustering using Attention-Based Neural Networks. December 2019. doi: 10.26434/chemrxiv.9897365.v2. URL https://chemrxiv.org/articles/Data-Driven_Chemical_Reaction_Classification_with_Attention-Based_Neural_Networks/9897365.
- Segler, M. H. S., Preuss, M., and Waller, M. P. Planning chemical syntheses with deep neural networks and symbolic AI. *Nature*, 555(7698):604–610, March 2018. ISSN 0028-0836, 1476-4687. doi: 10.1038/nature25978. URL <http://www.nature.com/doi/10.1038/nature25978>.
- Skoraczyski, G., Dittwald, P., Miasojedow, B., Szymku, S., Gajewska, E. P., Grzybowski, B. A., and Gambin, A. Predicting the outcomes of organic reactions via machine learning: are current descriptors sufficient? *Scientific Reports*, 7, June 2017. ISSN 2045-2322. doi: 10.1038/s41598-017-02303-0. URL <https://www.ncbi.nlm.nih.gov/pmc/articles/PMC5472585/>.
- Tokui, S., Oono, K., Hido, S., and Clayton, J. Chainer: a Next-Generation Open Source Framework for Deep Learning. 2015. URL <https://chainer-chemistry.readthedocs.io/en/latest/index.html>.
- Velickovi, P., Cucurull, G., Casanova, A., Romero, A., Li, P., and Bengio, Y. Graph Attention Networks. *arXiv:1710.10903 [cs, stat]*, February 2018. URL <http://arxiv.org/abs/1710.10903>. arXiv: 1710.10903.
- Weininger, D. SMILES, a chemical language and information system. 1. Introduction to methodology and encoding rules. *Journal of Chemical Information and Modeling*, 28(1):31–36, February 1988. ISSN 1549-9596. doi: 10.1021/ci00057a005. URL <https://pubs.acs.org/doi/abs/10.1021/ci00057a005>.
- Withnall, M., Lindelf, E., Engkvist, O., and Chen, H. Building attention and edge message passing neural networks for bioactivity and physical-chemical property prediction. *Journal of Cheminformatics*, 12(1), December 2020. ISSN 1758-2946. doi: 10.1186/s13321-019-0407-y. URL <https://jcheminf.biomedcentral.com/articles/10.1186/s13321-019-0407-y>.
- Wu, X.-Z. and Zhou, Z.-H. A Unified View of Multi-Label Performance Measures. *arXiv:1609.00288 [cs]*, September 2017. URL <http://arxiv.org/abs/1609.00288>. arXiv: 1609.00288.

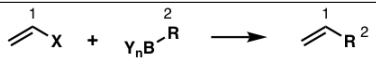
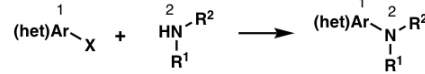
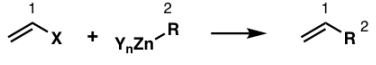
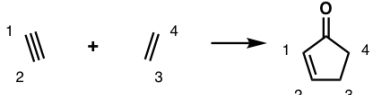
Supplementary Material: Graph Neural Networks for the Prediction of Organic Reaction Conditions

Serim Ryou ^{*1} Michael R. Maser ^{*2} Alexander Y. Cui ^{*3} Travis J. DeLano ² Yisong Yue ³ Sarah E. Reisman ²

S1. Data preparation

All datasets used herein were obtained from queries to the Reaxys database ([Reaxys](#)). Results from both journals and patents are included for all reaction types. An expanded Table 1 with depictions of the four reaction queries is shown in Table S1.

Table S1. Full summary of reaction sets studied with Reaxys query depictions.

name	query	reactions	bins	reactions/bin	categories
Suzuki		145,413	118	1232.3	5
CN		36,519	205	178.1	5
Negishi		6,391	105	60.9	5
PKR		2,749	83	33.1	8

For each reaction, the atoms involved in cross-coupling bond formation are enumerated in reactants and products, specified in the Reaxys queries *via* atom mapping. The number of reactions in Table S1 refers to counts after pre-processing. General pre-processing details used for all reactions are included below, followed by reaction-specific procedures. It should be noted that the four reactions modeled here share a similar format, typically containing one or two “coupling partners” (i.e. reactants) that react to form a single product upon treatment with a set of categorized conditions. In principle, the modeling framework described herein can be applied to any reaction format, provided a condition dictionary is written. Studies applying the current framework to reactions of other formats are currently ongoing.

General pre-processing. In all datasets, reactions without reactant or product structures, condition information, or reaction yields are removed unless otherwise specified. Duplicate condition information is removed such that each reaction contained only unique entries for each dictionary category (*vide infra*). It is possible that this duplicate information is meant to signify multiple equivalents of reaction components (i.e. stoichiometry), but given the unstructured nature of this feature in Reaxys, we do not consider it here. After trimming, condition entries are pooled and all unique values extracted with their frequency of appearance in the trimmed dataset to construct the full length reaction dictionary. The dictionary is truncated at a cumulative 95% coverage of instance frequencies. This serves to avoid both sparsity in label bins and unreasonably lengthy curation. All resulting entries are assigned an identifier for their reaction role, which we term categories. The dictionaries are then sorted into categories for further processing. Reagents that could serve multiple reaction roles are assigned each plausible identifier and copied into each respective category.

Once categorized, the frequencies of each bin are recalculated within the category, and each category is again truncated at 95% total coverage. At the data scale studied here, reagent bins outside of this threshold typically appear in the dataset under

10 times total. We therefore exclude them to avoid unnecessary dimensionality in the label space and reduce overfitting. Even still, class-imbalance within the categories is pronounced (Cui et al., 2019), as evidenced by the “long-tail” distributions provided in Section S4. Categories are combed to identify any bins with unique names that refer to the same reagent, often by misspelling, abbreviation, etc. At this stage, all unique species are assigned a bin label within their category, and the categories are recombined. This constitutes the final reaction dictionary and defines the label space for our prediction task. Appropriate categories were also assigned “null” bins to indicate reactions not specifying labels in that category.

Additional Suzuki pre-processing. The initial export contained 154,634 data points at time of download. Reactions without yields (~1,500) or solvent (~2,700) were removed. Reactions with more or less than 2 reactants, and more than one product (~6,800) were removed. The final dataset contained 145,413 reactions with a dictionary of 118 bins in the categories metal (M), ligand (L), base (B), solvent (S), and additive (A). Roughly 25% of reactions did not have temperatures specified, so this feature was dropped.

Additional CN pre-processing. The initial export contained 39,902 data points at time of download. Reactions without solvent were retained, as this dataset included non-catalytic CN couplings such as S_NAr reactions, often run in the neat amine reactant. Reactions with more or less than 2 reactants and 1 product (~3,000) were removed. Reactions with more than 4 reagents (~250) were removed. The final dataset contained 36,519 reactions with a dictionary of 205 bins in the categories metal (M), ligand (L), base (B), solvent (S), and additive (A). Roughly 30% of reactions did not have temperatures specified, so this feature was dropped.

Additional Negishi pre-processing. The initial export contained 11,388 data points at time of download. Reactions without yields (~3,500) or solvent (~350) were removed. Reactions with more than 2 reactants, 3 solvents, and/or 4 reagents (~1,200) were removed. The final dataset contained 6,391 reactions with a dictionary of 105 bins in the categories metal (M), ligand (L), temperature (T), solvent (S), and additive (A). Almost 90% of reactions had temperatures specified, so this feature was retained. Those with unspecified temperatures were assumed to occur ambiently and assigned as 20 C.

Additional PKR pre-processing. The initial export contained 4,275 data points at time of download. Both inter- and intramolecular reactions were retained, so reactions contained either 1 or 2 reactants. Reactions without yields (~1,000) were removed. Reactions with more than 2 reactants, 3 solvents, and/or 4 reagents (~500) were removed. The final dataset contained 2,749 reactions with a dictionary of 83 bins in the categories metal (M), ligand (L), temperature (T), solvent (S), additive (O), activator (A), gas (G), and pressure (P). The gas category is a binary identifier for the use of a carbon monoxide (CO) atmosphere.

S2. Computational details and hyperparameters

All neural network (NN) architectures tested herein were used directly from the Chainer Chemistry (ChainerChem) library (Tokui et al., 2015), modified only as needed to fit each dataset task. In all cases, a graph processing network (GPN) was selected and combined with a dense multi-layer perceptron (MLP), which were trained together as a joint network. All models were trained for 100 epochs on 1 NVIDIA K80 GPU device, unless otherwise specified. Training and test sets were held consistent between models for each reaction dataset. This was done by first splitting each dataset into 90/10 train/test, then splitting the training set into 90/10 train/validation, resulting in a final split of 81/9/10 train/validation/test overall. A dummy predictor that always predicts the most frequent bin in each label category was also created for each dataset as a baseline performance reference.

General parameters and default hyperparameter settings are summarized in Table S2, which are held constant across all models and datasets unless otherwise specified in Table S3. Every attempt was made to keep shared hyperparameters consistent between model types, and the majority were set to defaults. However, there were certain cases where this resulted in excessive memory requirements and crashes during model training. To adapt to these cases, parameters such as the hidden dimension (hidden_dim) were incrementally decreased until training was successful. These cases are noted in Table S3.

Model names listed follow those from original references (see main text), names in parentheses refer to those used by Chainer functions. It should be noted that while the predicted vectors contain a single label from each category, it is possible that the ground truth contains more than one or zero. We add a null label to each sub-dictionary to handle the zero case, and with multiple ground truths we treat a category's prediction as accurate if any are correctly identified. The null case was found commonly in ligand and additive categories, where a null ligand often resulted from use of a pre-ligated metal source. The multi-output scenario arose most frequently in the form of mixed solvent systems.

Table S2. Computational details and general parameters used for all models.

parameter	value	description
loss	sigmoid cross entropy	loss function used for training
optimizer	Adam	model optimization algorithm
train/valid/test	81/9/10	data splitting
batch size	32	batch size used for gradient calculations
epochs	100	number of training epochs
out_dim	128	number of units in the readout
hidden_dim	128	number of units in the hidden layers
n_layers	4	number of convolutional layers
n_atom_types	117	number of allowed atom types
concat_hidden	False	readouts concatenated at each layer

Table S3. Additional model-specific hyperparameter settings.

model	hyperparameter	value	description
NFP	max_degree	6	max degree of atom nodes in the graph
GGNN	weight_tying	True	use weight tying
	num_edge_type	4	edge (i.e. bond) types allowed (4 includes single, double, triple and aromatic)
MPNN	weight_tying	True	use weight tying
	message_func	'edgenet'	message function
	readout_func	'set2set'	readout function
	hidden_dim	16	default 128 required excessive memory
	batch size	8	default 32 required excessive memory
	epochs	32 & 5	Suzuki & CN; memory errors found at higher epochs; validation loss had converged
Weave (WeaveNet)	weave_channels	200	weave channel dimensionality
	n_atom	20	number of atoms in input arrays
	n_sub_layer	1	number of layers in each pairing layer
	readout_mode	'sum'	readout mode
	epochs	10	Suzuki only; memory errors found at higher epochs; validation loss had converged
R-GAT (RelGAT)	n_heads	3	number of multi-head attentions
	negative_slope	0.2	LeakyRELU negative angle
	dropout_ratio	-1.	dropout for normalized attention coefficients
	softmax_mode	across	method for taking softmax over logits
	concat_heads	False	concatenate multi-head attentions
	weight_tying	False	use weight tying
	hidden_dim	12	default 128 required excessive memory
R-GCN (RelGCN)	out_channels	128	output feature vector dimensionality
	ch_list	None	channels in update layers
	input_type	'int'	input vector type
	scale_adj	True	normalize adjacency matrix
RS-GCN (RSGCN)	use_batch_norm	False	apply batch normalization after convolutions
	readout	None	readout mode (None defaults to 'sum')
	dropout_ratio	0.5	dropout function ratio
MLP	out_dim	class_num	custom for number of classes in each dataset
	n_layers	2	number of dense layers
	activation	relu	activation function

S3. Expanded results

Modeling results for top-3 rankings are included below in Table S4. It should be noted that since the “CO (g)” category in the PKR dataset is a binary class (either yes or no), the top-3 accuracy will always be 1. This category is therefore excluded from AER calculations for this section.

Table S4. Summary of top-3 ranking accuracies for all architectures across the four datasets.

reaction	category	dummy	NFP	GGNN	MPNN	Weave	R-GAT	R-GCN	RS-GCN
Suzuki	AER	-	0.3615	0.3491	0.0451	0.0847	0.2641	0.4936	0.2732
	metal	0.6744	0.8198	0.7935	0.7298	0.7388	0.7792	0.8482	0.7701
	ligand	0.9269	0.9542	0.9555	0.9292	0.9351	0.9474	0.9644	0.9524
	base	0.7344	0.7795	0.7693	0.7337	0.7366	0.7603	0.8123	0.7564
	solvent	0.8013	0.8484	0.8430	0.7948	0.8055	0.8265	0.8836	0.8169
	additive	0.9771	0.9904	0.9919	0.9784	0.9790	0.9884	0.9934	0.9899
CN	AER	-	0.4615	0.5240	0.0647	0.2077	0.3802	0.5391	0.3785
	metal	0.6526	0.8170	0.8392	0.6795	0.7393	0.7981	0.8479	0.7734
	ligand	0.6647	0.8222	0.8532	0.6934	0.7203	0.7970	0.8605	0.7992
	base	0.6400	0.8142	0.8326	0.6827	0.7360	0.7858	0.8452	0.7964
	solvent	0.5677	0.7532	0.7847	0.5885	0.6538	0.7211	0.7973	0.7129
	additive	0.9156	0.9537	0.9564	0.9151	0.9288	0.9433	0.9534	0.9471
Negishi	AER	-	0.6503	0.6722	0.0896	0.2590	0.3598	0.6590	0.5148
	metal	0.5008	0.8054	0.8485	0.5072	0.6045	0.6715	0.8086	0.7512
	ligand	0.8549	0.9601	0.9506	0.8724	0.8947	0.9187	0.9522	0.9474
	temperature	0.5885	0.8262	0.8740	0.6619	0.7624	0.7608	0.8517	0.8086
	solvent	0.8788	0.9522	0.9569	0.8852	0.9059	0.9171	0.9537	0.9394
	additive	0.9043	0.9745	0.9681	0.9123	0.9203	0.9314	0.9761	0.9426
PKR	AER	-	0.5957	0.6861	0.2695	0.3336	0.2947	0.6844	0.5063
	metal	0.7132	0.8604	0.8717	0.7849	0.8302	0.8189	0.9057	0.8604
	ligand	0.9019	0.9887	0.9849	0.9811	0.9736	0.9736	0.9849	0.9887
	temperature	0.5962	0.8038	0.8792	0.6415	0.6981	0.6604	0.8528	0.7509
	solvent	0.5925	0.8340	0.8981	0.6981	0.7472	0.6981	0.8679	0.8226
	activator	0.8830	0.9660	0.9698	0.8755	0.8906	0.8792	0.9774	0.9283
	CO (g)	1.0000	1.0000	1.0000	1.0000	1.0000	1.0000	1.0000	1.0000
	additive	0.9321	0.9698	0.9736	0.9472	0.9660	0.9509	0.9698	0.9736
	pressure	0.9623	0.9774	0.9849	0.9736	0.9623	0.9736	0.9849	0.9698

S4. Exploratory data analysis (EDA)

A statistical analysis of the chemical space and reaction dictionary was conducted for each dataset. The analysis included distributions of reaction yields, categorical label frequencies, and the following 16 molecular descriptors of reaction products calculated with RDKit ([Open-Source, 2006](#)):

1. MolWt = molecular weight (g/mol)
2. MolLogP = molecular logP (lipophilicity measure)
3. TPSA = topological polar surface area (\AA^2)
4. HeavyAtomCount = number of non-H atoms

5. NumHeteroatoms = number of heteroatoms (non-H or C)
6. NumValenceElectrons = number of valence electrons
7. NumHAcceptors = number of hydrogen-bond acceptors
8. NumHDonors = number of hydrogen-bond donors
9. NumRotatableBonds = number of rotatable bonds
10. RingCount = number of rings
11. NumAromHeterocycles = number of aromatic heterocycles (aromatic rings with at least one non-C atom)
12. NumAromCarbocycles = number of aromatic carbocycles (aromatic rings made entirely of C atoms)
13. NumSatHeterocycles = number of saturated heterocycles (saturated rings with at least one non-C atom)
14. NumSatCarbocycles = number of saturated carbocycles (saturated rings made entirely of C atoms)
15. FractionCSP3 = fraction of atoms sp^3 -hybridized
16. QED = quantitative estimation of drug-likeness

Note: The descriptor names above are not all exactly as written in their respective RDKit functions. For the figures, the property distributions were truncated at the 1st and 99th percentile in each dataset analysis to avoid sparsity. The full span of the distributions is reflected in the summary tables. For full code, see the EDA jupyter notebooks in the associated GitHub repository.

Suzuki dataset.

Table S5. Summary of product molecular properties in Suzuki dataset.

	Yield	MolWt	MolLogP	TPSA	HeavyAtomCount	NumHeteroatoms	NumValenceElectrons
count	145413	144972	144972	144972	144972	144972	144972
mean	0.682	352.072	4.704	49.805	25.323	4.938	129.042
std	0.237	146.421	2.258	36.775	10.435	3.421	54.925
min	0	82.106	-5.969	0	6	0	32
25%	0.53	233.227	3.354	20.23	17	2	84
50%	0.73	331.757	4.142	43.6	24	4	120
75%	0.88	438.444	5.519	72.45	31	7	160
max	1	2339.16	46.845	472.09	164	86	952

	NumHAcceptors	NumHDonors	NumRotatableBonds	RingCount	NumAromHeterocycles
count	144972	144972	144972	144972	144972
mean	3.622	0.525	3.968	3.472	1.028
std	2.589	0.832	3.483	1.639	1.05
min	0	0	0	0	0
25%	2	0	2	2	0
50%	3	0	3	3	1
75%	5	1	5	4	2
max	39	16	115	11	8

	NumAromCarbocycles	NumSatHeterocycles	NumSatCarbocycles	FractionCSP3	QED
count	144972	144972	144972	144972	144972
mean	1.976	0.171	0.097	0.188	0.544
std	1.248	0.45	0.394	0.166	0.201
min	0	0	0	0	0.008
25%	1	0	0	0.067	0.396
50%	2	0	0	0.143	0.591
75%	2	0	0	0.3	0.695
max	9	7	5	1	0.948

Figure S1. Distribution of reaction yields in Suzuki dataset.

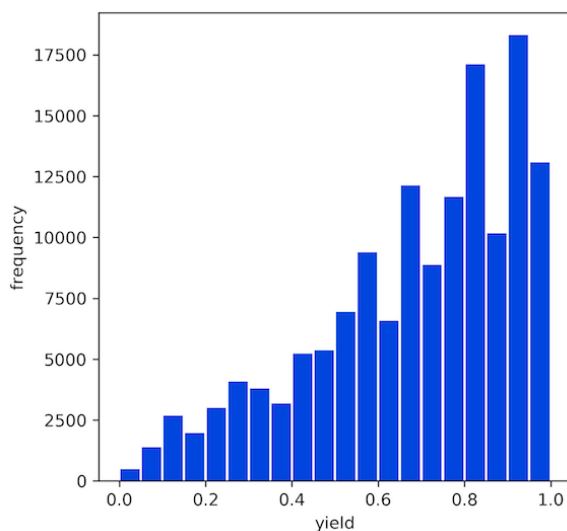


Figure S2. Distribution of each molecular descriptor in Suzuki dataset products.

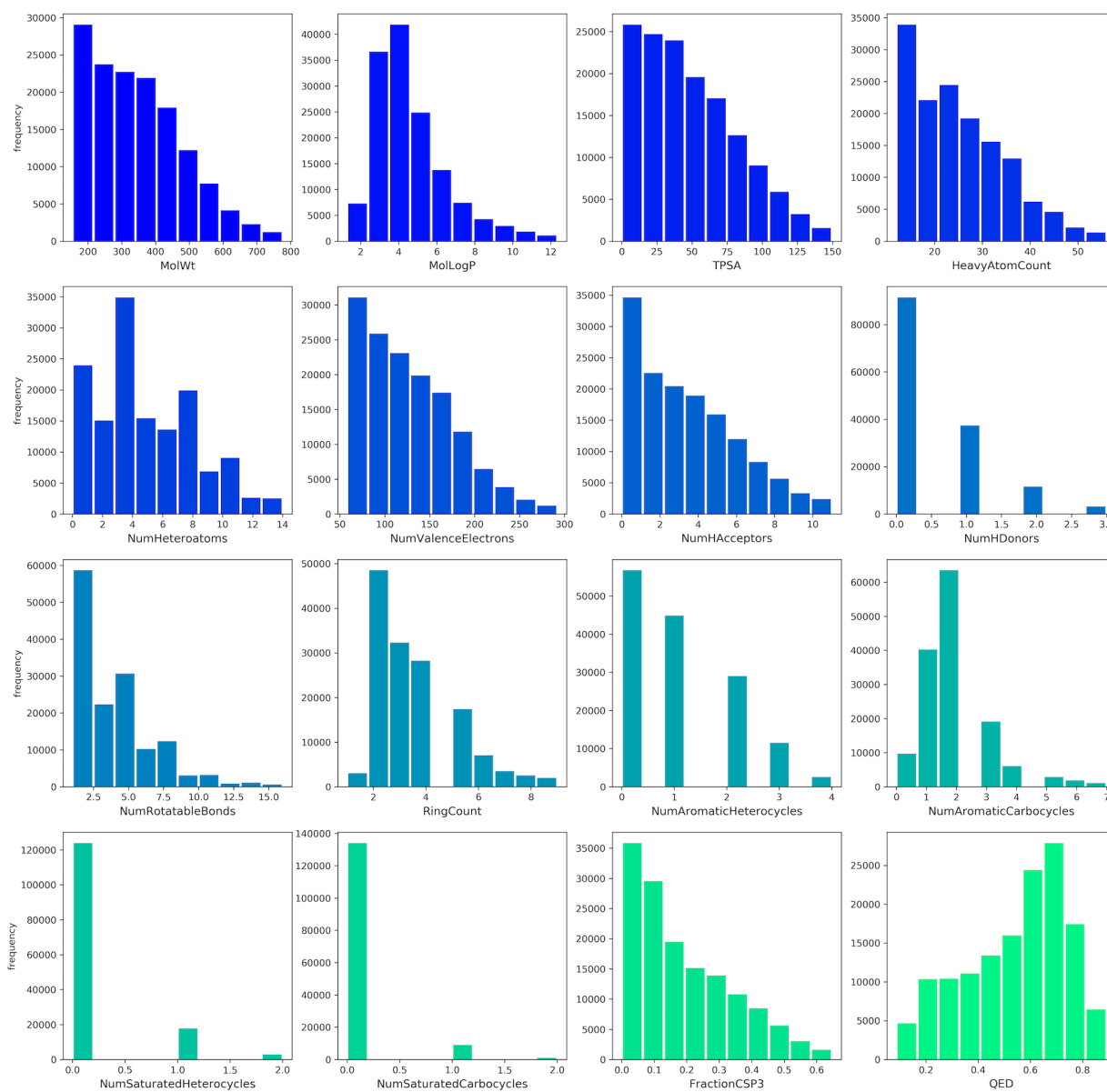
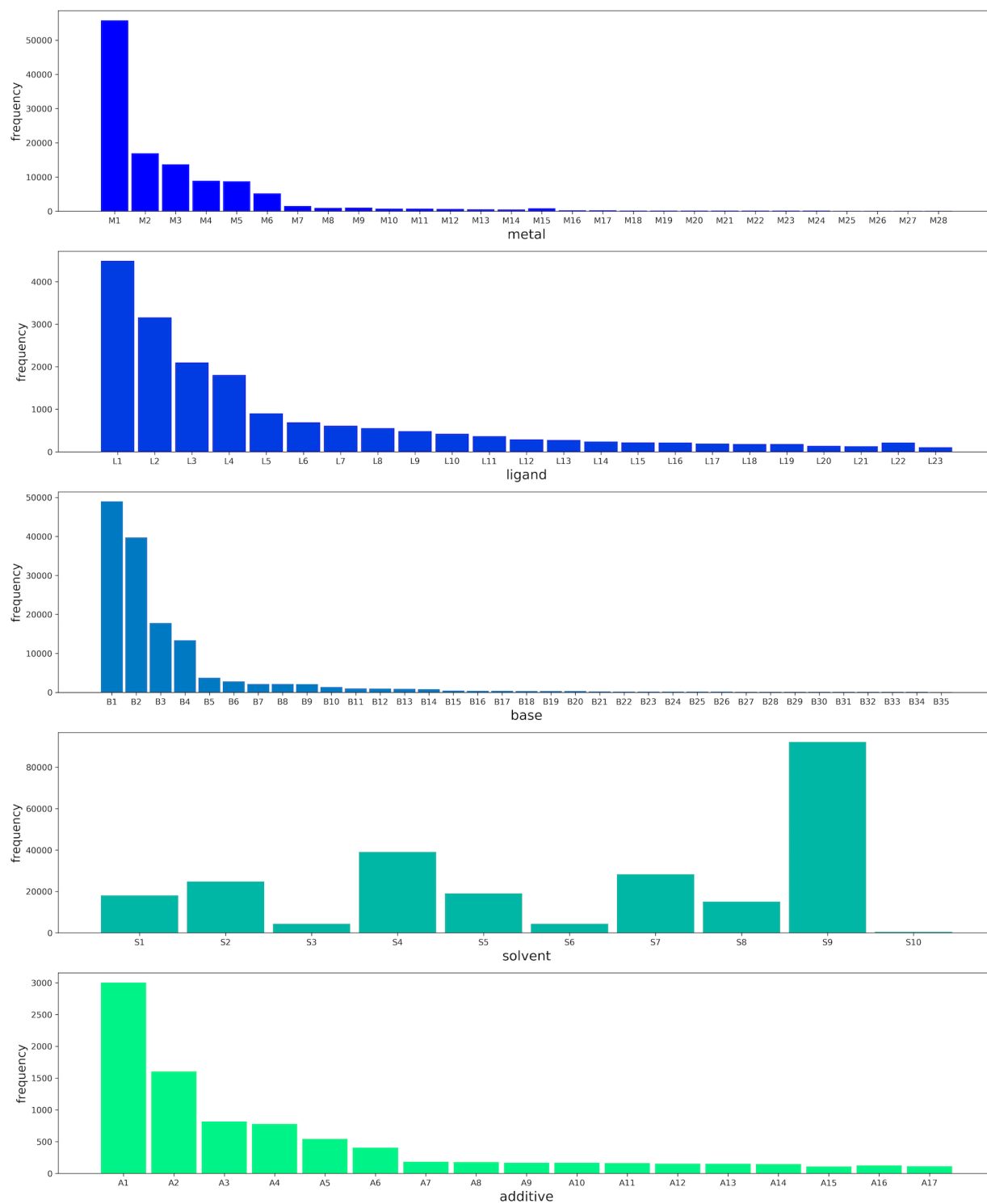


Figure S3. Distribution of dictionary bin frequencies in Suzuki dataset.



CN dataset.

Table S6. Summary of product molecular properties in CN dataset.

	Yield	MolWt	MolLogP	TPSA	HeavyAtomCount	NumHeteroatoms	NumValenceElectrons
count	36519	36504	36504	36504	36504	36504	36504
mean	0.699	310.3	4.281	41.023	22.272	4.237	114.149
std	0.229	123.812	2.279	32.613	8.887	2.82	44.884
min	0	107.156	-1.441	3.01	8	1	42
25%	0.57	216.24	2.87	12.47	16	2	82
50%	0.75	279.325	3.763	33.2	20	4	102
75%	0.88	376.4	5.166	58.44	27	6	136
max	1	2527.86	30.826	355.67	172	40	960

	NumHAcceptors	NumHDonors	NumRotatableBonds	RingCount	NumAromHeterocycles
count	36504	36504	36504	36504	36504
mean	3.128	0.673	3.598	3.022	0.452
std	2.018	0.771	2.804	1.643	0.691
min	1	0	1	1	0
25%	2	0	2	2	0
50%	3	1	3	3	0
75%	4	1	5	4	1
max	39	8	114	12	7

	NumAromCarbocycles	NumSatHeterocycles	NumSatCarbocycles	FractionCSP3	QED
count	36504	36504	36504	36504	36504
mean	2.093	0.292	0.067	0.225	0.603
std	1.292	0.53	0.361	0.191	0.197
min	1	0	0	0	0.015
25%	1	0	0	0.067	0.481
50%	2	0	0	0.182	0.647
75%	2	1	0	0.4	0.757
max	9	4	5	0.917	0.948

Figure S4. Distribution of reaction yields in CN dataset.

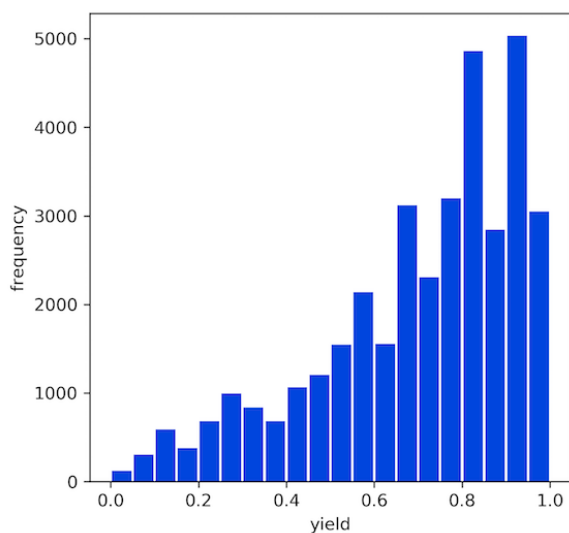


Figure S5. Distribution of each molecular descriptor in CN dataset products.

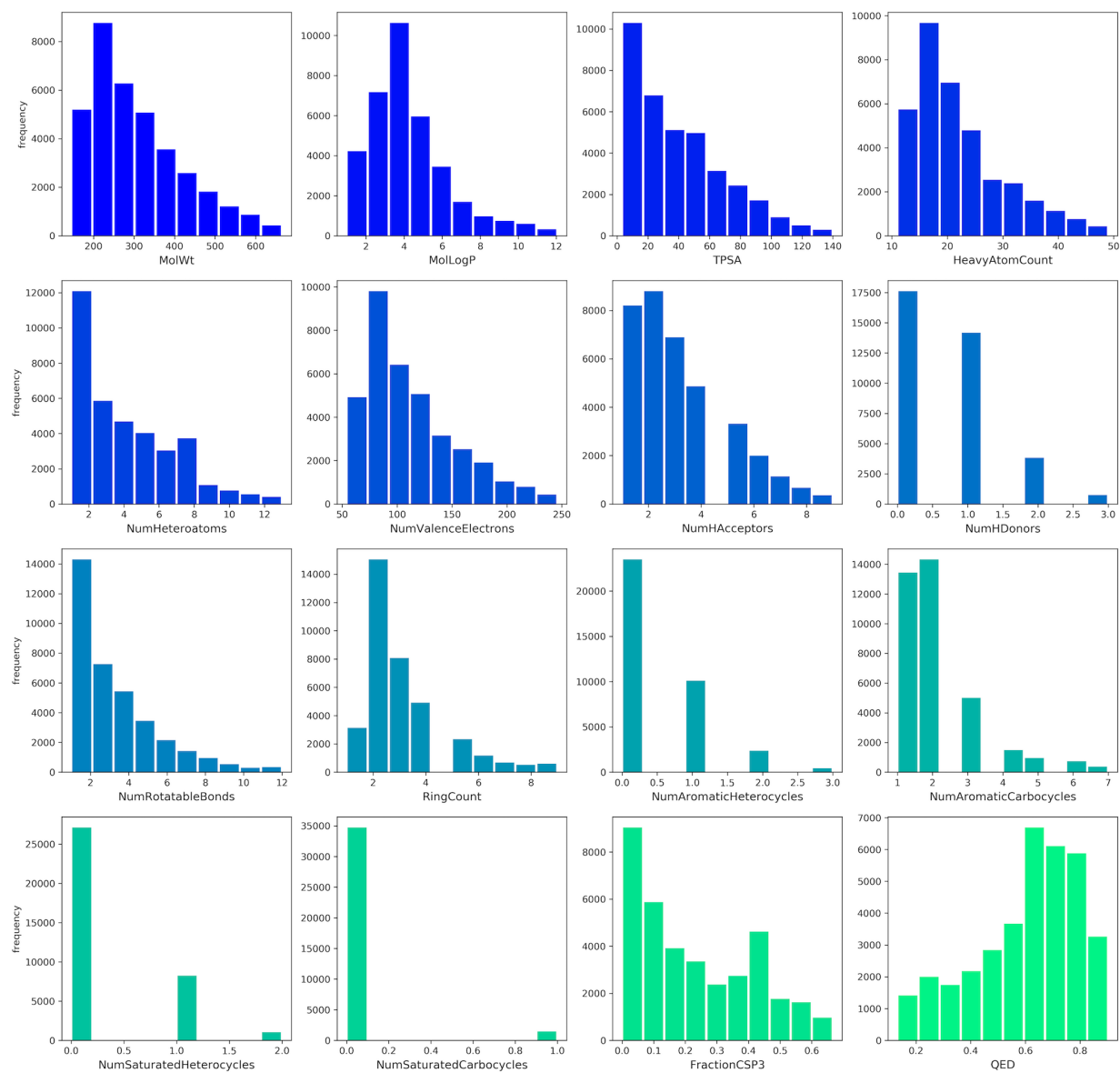
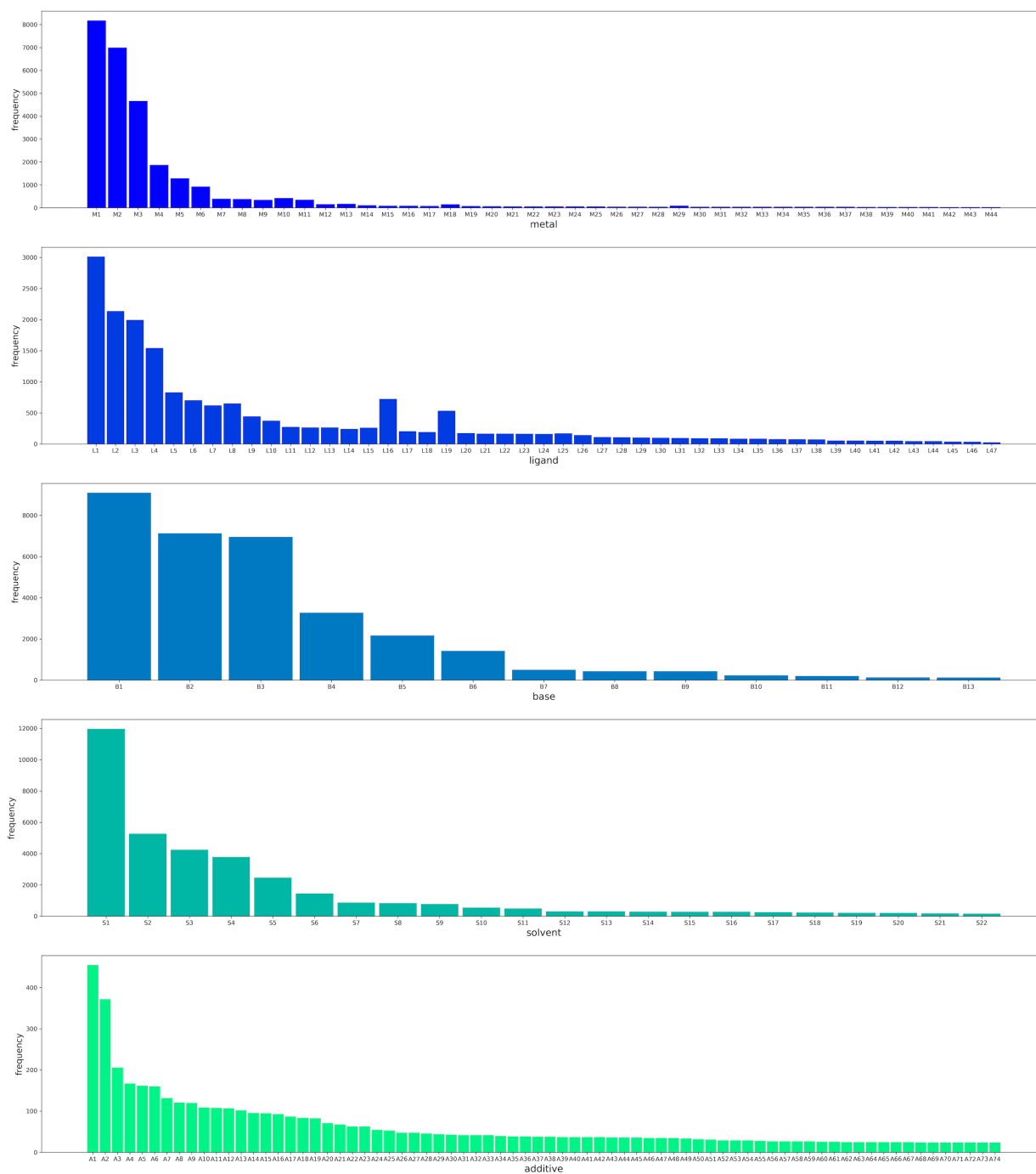


Figure S6. Distribution of dictionary bin frequencies in CN dataset.



Negishi dataset.

Table S7. Summary of product molecular properties in Negishi dataset.

	Yield	MolWt	MolLogP	TPSA	HeavyAtomCount	NumHeteroatoms	NumValenceElectrons
count	6391	6383	6383	6383	6383	6383	6383
mean	0.711	288.295	3.888	39.464	20.4	3.92	106.51
std	0.219	111.961	1.677	28.719	7.858	2.679	42.459
min	0.005	82.102	-1.691	0	6	0	32
25%	0.59	209.248	2.815	18.46	15	2	76
50%	0.76	263.243	3.639	35.53	19	3	98
75%	0.889	339.369	4.651	55.14	24	5	126
max	1	1209.1	17.401	213.58	80	28	456

	NumHAcceptors	NumHDonors	NumRotatableBonds	RingCount	NumAromHeterocycles
count	6383	6383	6383	6383	6383
mean	2.867	0.246	3.599	2.344	0.68
std	1.992	0.53	2.823	1.238	0.824
min	0	0	0	0	0
25%	1	0	2	2	0
50%	3	0	3	2	0
75%	4	0	5	3	1
max	17	6	31	9	5

	NumAromCarbocycles	NumSatHeterocycles	NumSatCarbocycles	FractionCSP3	QED
count	6383	6383	6383	6383	6383
mean	1.224	0.134	0.149	0.297	0.615
std	0.915	0.392	0.494	0.213	0.17
min	0	0	0	0	0.036
25%	1	0	0	0.118	0.529
50%	1	0	0	0.273	0.649
75%	2	0	0	0.45	0.741
max	7	4	4	0.943	0.946

Figure S7. Distribution of reaction yields in Negishi dataset.

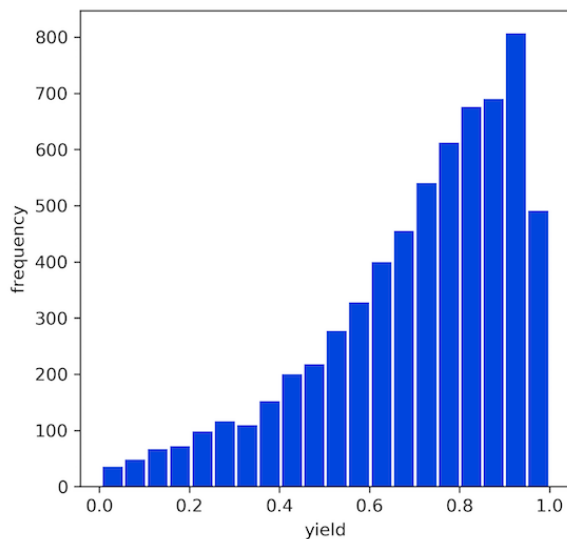


Figure S8. Distribution of each molecular descriptor in Negishi dataset products.

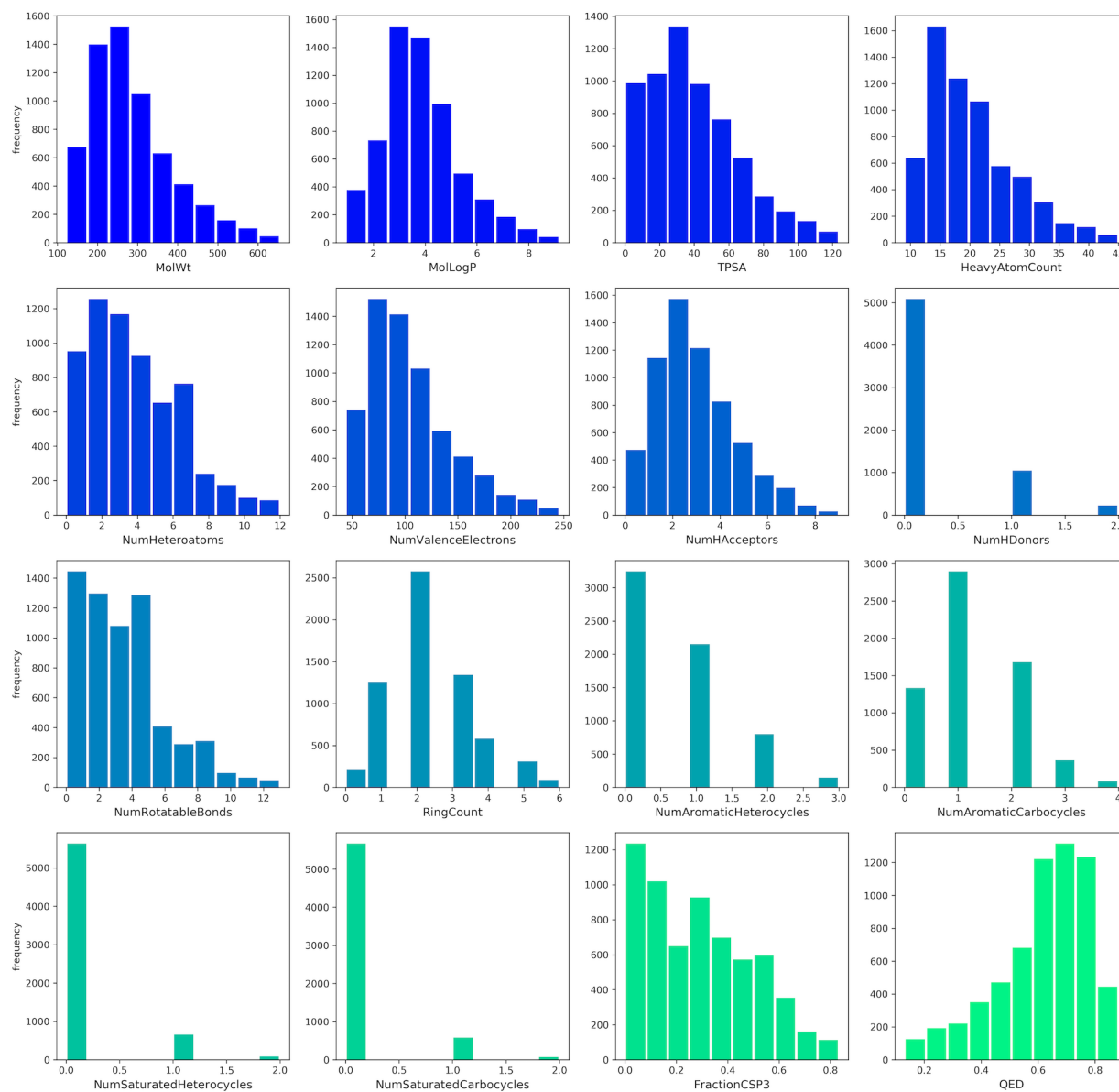
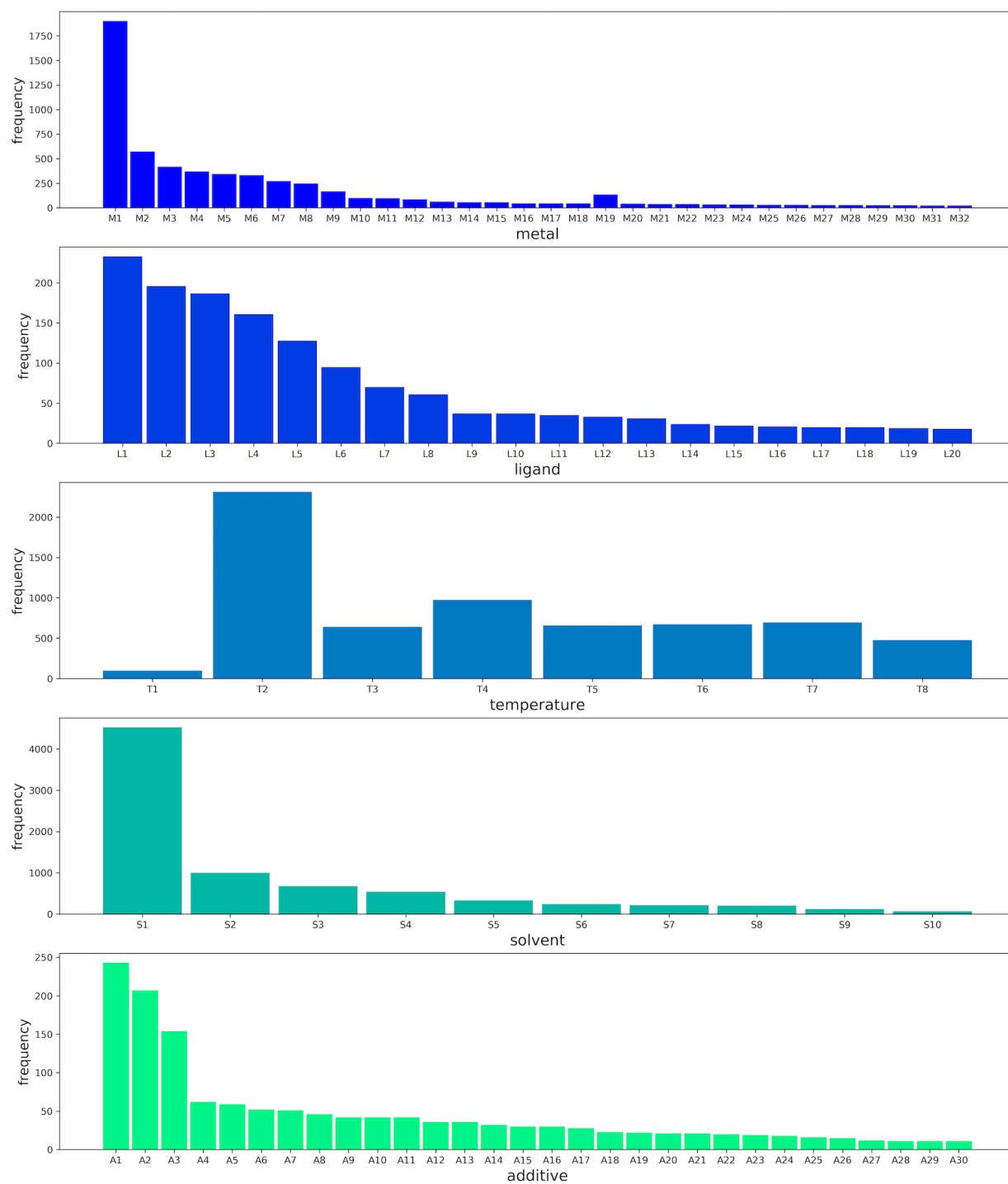


Figure S9. Distribution of dictionary bin frequencies in Negishi dataset.



PKR dataset.

Table S8. Summary of product molecular properties in PKR dataset.

	Yield	MolWt	MolLogP	TPSA	HeavyAtomCount	NumHeteroatoms	NumValenceElectrons
count	2749	2746	2746	2746	2746	2746	2746
mean	0.662	312.949	3.399	45.976	22.334	3.997	117.857
std	0.218	94.145	1.705	23.243	6.508	1.992	34.337
min	0.03	122.167	-1.182	0	9	0	48
25%	0.51	240.302	2.096	26.3	17	2	92
50%	0.69	303.393	3.125	44.76	22	4	114
75%	0.84	364.4	4.374	63.68	26	5	136
max	1	905.243	11.217	151.35	64	13	340

	NumHAcceptors	NumHDonors	NumRotatableBonds	RingCount	NumAromHeterocycles
count	2746	2746	2746	2746	2746
mean	3.146	0.111	3.038	3.26	0.047
std	1.643	0.347	2.357	1.085	0.216
min	0	0	0	1	0
25%	2	0	1	3	0
50%	3	0	3	3	0
75%	4	0	4	4	0
max	13	3	24	8	2

	NumAromCarbocycles	NumSatHeterocycles	NumSatCarbocycles	FractionCSP3	QED
count	2746	2746	2746	2746	2746
mean	0.959	0.425	0.538	0.472	0.636
std	0.983	0.64	0.713	0.203	0.153
min	0	0	0	0	0.051
25%	0	0	0	0.308	0.555
50%	1	0	0	0.45	0.663
75%	1	1	1	0.643	0.747
max	5	4	4	0.929	0.924

Figure S10. Distribution of reaction yields in PKR dataset.

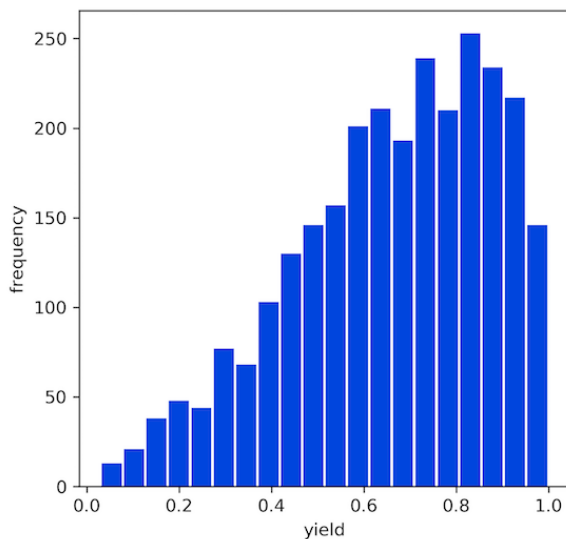


Figure S11. Distribution of each molecular descriptor in PKR dataset products.

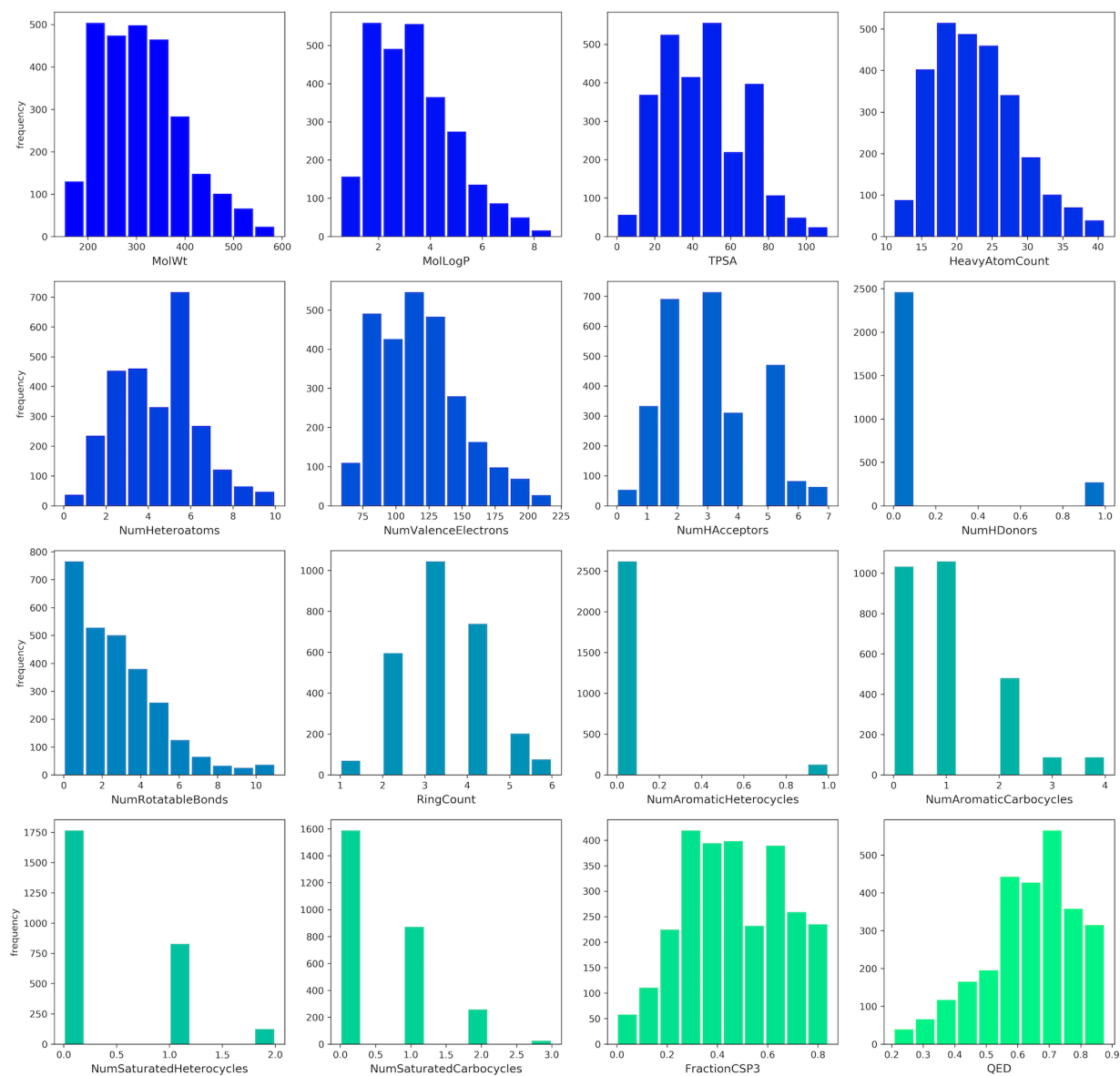


Figure S12. Distribution of dictionary bin frequencies in PKR dataset.

